

IMECE2004-61291

MICROSTRUCTURE EVOLUTION DURING ALTERNATING-CURRENT-INDUCED FATIGUE*

R. R. Keller, R. H. Geiss, Y. -W. Cheng, and D. T. Read

Materials Reliability Division
National Institute of Standards and Technology
Boulder, CO 80305

ABSTRACT

Subjecting electronic interconnect lines to high-density, low-frequency alternating current creates cyclic thermomechanical stresses that eventually cause electrical failure. A detailed understanding of the failure process could contribute to both prevention and diagnostics. We tested unpassivated Al-1Si traces on the NIST-2 test chip; these are 3.5 μm wide by 0.5 μm thick by 800 μm long, with a strong (111) as-deposited fiber texture and an initial average grain diameter of approximately 1 μm . We applied rms current densities of 11.7 to 13.2 MA/cm² at 100 Hz. Resistance changes in the lines indicated that such current densities produce temperature cycles at 200 Hz with amplitude exceeding 100 K. Open circuits occurred in under 10 minutes, with substantial surface damage seen after only one minute. A few failures initiated at lithography defects initially present in the lines, but most were produced by the current alone. In one detailed example presented in this paper, we monitored the damage process by interrupting the current at 10, 20, 40, 80, 160, and 320 s in order to characterize an entire line by scanning electron microscopy and automated electron backscatter diffraction (EBSD); failure took place after 697 s. Results are described in terms of deformation, grain growth, and orientation changes.

INTRODUCTION

Virtually any multi-material system subjected to temperature cycles will undergo thermomechanical fatigue, due to mismatches in coefficients of thermal expansion among the materials comprising the system. Since small-scale structures such as those found in microelectronic circuits and micro-electromechanical systems tend to be composed of many dissimilar materials, they are prime candidates for this type of wear-out mechanism. In general, though, mechanical properties and behaviors of such materials are not easily predictable by

extrapolating from known bulk behavior [1]. There are two strong reasons for this. First, in small-scale structures, microstructures are distinctly different from those seen in bulk materials of the same chemical composition; therefore, defect behavior during deformation is very different. Second, what might be considered a small amount of surface damage in bulk materials can be very near to catastrophic failure in systems composed of many material interfaces in very close proximity; therefore, failure criteria will be different. We expect the second issue to be particularly important for cyclic deformation, where plastic strain can be far more localized than that associated with monotonic straining of bulk materials [2].

Considerable work addressing dislocation behavior during monotonic straining of thin films and other small structures can be found, e.g. [3]. Dehm and Arzt studied dislocation activity associated with the initial few cycles of a thermal test within a transmission electron microscope [4]. Some detailed studies of both low- and high-cycle mechanical fatigue of free-standing films and films on flexible substrates [5] have been reported by Schwaiger and co-workers. Aside from these examples, there is in general little work addressing microstructural aspects of fatigue in such structures, and less work yet on thermomechanical fatigue in either the low-cycle or high-cycle regimes. Wafer-curvature measurements of stress during thermal cycling are common in the thin film industry [6], but these are impractical for probing more than a few tens of cycles.

Alternating current-based tests, under conditions of low frequency and high current density, offer an alternative, promising method for conducting thermomechanical fatigue evaluations of small-scale structures into the low- or high-cycle regime [7]. The tests are based on the principle that within each half cycle of current, Joule heating of the current-carrying segment causes not only that segment, but also the surrounding materials to heat up. Heat flow in materials that typically

*Contribution of U.S. Department of Commerce;
not subject to copyright.

comprise a microelectronic device is rapid enough to allow for nearly complete dissipation by the start of the next half cycle. Calibrations of resistivity against temperature then allow for a reasonable estimate of the cyclic temperature behavior [7], which can be used in assessing cyclic strain and stress. To the best of our knowledge, this is the only method so far developed that is capable of testing thermomechanical fatigue behavior of small-scale structures to large numbers of cycles in the materials' in-use conditions, e.g., patterned thin film metallizations on a silicon-based substrate, in either a passivated or unpassivated state.

While stresses are usually greater in small-scale structures than in bulk materials, fatigue lifetime behavior is qualitatively similar. Namely, the number of cycles to AC-induced failure decreases as the cyclic stress or strain amplitude increases [8]. Complete details of the microstructural changes during AC-induced thermomechanical fatigue of thin films, however, have not yet been fully documented. In this paper, we build on work presented in reference [9], which documented early stages of damage formation, by presenting an evaluation of microstructure at later stages of AC-induced fatigue, through failure.

EXPERIMENTAL

AC tests were carried out on unpassivated, single-level structures composed of patterned and etched Al-1Si lines on oxidized silicon. We used a NIST-2 test structure originally designed for electromigration and thermal conductivity measurements. The lines were 800 μm long, 3.3 μm wide, and 0.5 μm thick. Current and voltage taps were present at each end of a given line, as shown in Figure 1. The current probes supplied the current and the voltage probes measured the potential drop across each test line, from which the electrical resistance was calculated. The measured resistances of 24 test lines, prior to testing, ranged from 13.77 to 14.13 Ω with an average of 13.89 Ω and an uncertainty of 0.01 Ω .

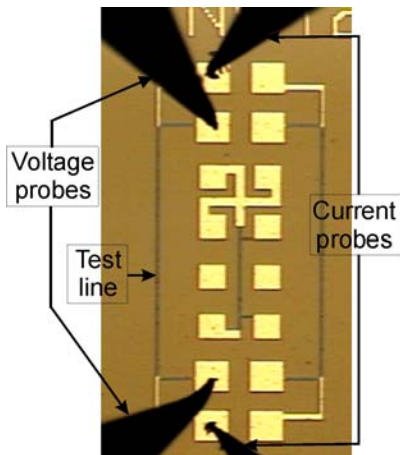


Figure 1. Low magnification optical microscope image of a NIST-2 test structure with four probes in place for electrical testing.

Testing was conducted using 100 Hz sinusoidal alternating currents with zero DC offset. Current was supplied with a current calibrator, which was driven by an arbitrary waveform generator. Current densities reported in this paper refer to rms current, and lifetimes refer to the time between the start of the test and open circuit. The test chip, having dimensions of 11 mm long, 9 mm wide, and 0.3 mm thick, was held in place on a steel stage during testing using a vacuum chuck. Lifetime tests were conducted continuously without interruption until the test lines became electrically open. During tests, the two voltage probes were removed from contacting the pads and changes of electrical resistance were not monitored.

Microstructure evolution during the course of one particular test was monitored using field emission scanning electron microscopy (FE-SEM) and automated electron backscatter diffraction (EBSD). For that particular specimen, a current density of 12.2 MA/cm² was applied. The average specimen temperature, as monitored using a thermocouple attached directly to the die, indicated a rise of < 10 K during electrical testing. However, the low-frequency AC signals led to temperature cycling superimposed onto the average die temperature, with amplitude of approximately 100 K, at a frequency of 200 Hz [8], which corresponds to the power cycling input into the line. We collected FE-SEM and EBSD data from the entire line prior to any testing, to establish the as-deposited condition. The line was then subjected to testing for 10 s and removed from the probe station for another series of EBSD measurements. The line was then subjected to another 10 s of testing, and so on. In this manner, we collected FE-SEM and EBSD data after the following accumulated time increments (in seconds): 0, 10, 20, 40, 80, 160, and 320. The specimen failed at 697 s. We note that this series of testing completes the initial monitoring of microstructure through 40 s, as reported in [9]. EBSD measurements were made using an accelerating voltage of 15 kV and electron beam step increments of 200 nm. Scan times were typically less than 5 minutes for the collection of 1800 points with 8x8 binning. All EBSD orientation maps are shown in the as-collected state, with no software-imposed filtering or clean-up algorithms applied.

RESULTS

Figure 2 shows the lifetime to open circuit as a function of nominal current density (current divided by initial cross-sectional area of the line). The trend is as expected, namely, increased current density decreases lifetime. We note that the lifetime of the specimen tested under interrupted conditions (shown in red), for microstructure observation, is shorter than that of specimens tested continuously to failure. This is likely due to a lower average temperature occurring during the interrupted test, since there was insufficient time for the chip to reach thermal equilibrium. However, the temperature amplitude should be unchanged in these two conditions.

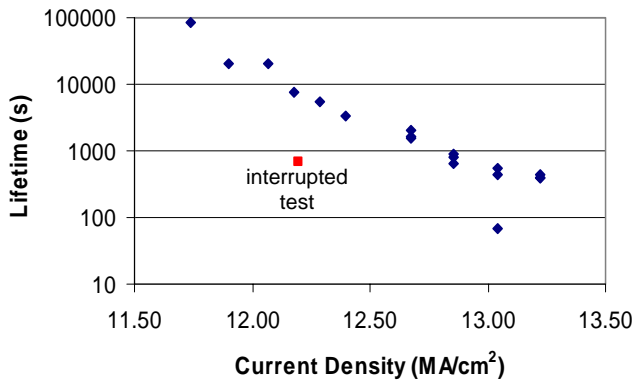


Figure 2. Time to open circuit versus applied current density. Data point from interrupted test shown in red.

SEM imaging revealed the development of severe topography on the initially smooth surfaces of the Al-1Si lines. Figure 3 shows an example of this damage evolving over time. The images are taken from the same regions of the same line, after interruption of the test at the times indicated. Within the first minute, damage develops in the form of surface wrinkling. The morphology of the wrinkling is reminiscent of that induced by the glide of dislocations intersecting the surface of a deformed metal. The damage becomes progressively more severe with increased stressing, leading up to very dramatic topography as shown in the bottom image of Figure 3. The open circuit event occurred elsewhere in that line, but also in the vicinity of very severe damage.

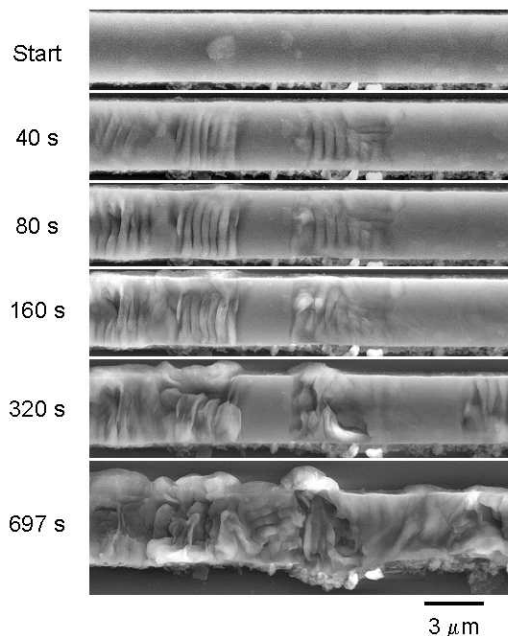


Figure 3. SEM series showing development of severe topography with accumulating AC test time. The line developed an open circuit at 697 s, at a different location.

We point out also the selectivity in damage formation. Figure 3 shows further that even through 320 s of testing (about half the time to open circuit), there are still regions of the line surface that appear to be smooth. Images from other areas of this line show several similar smooth regions, even after the line went to open circuit. In general, the proportion of damaged to smooth surface areas seems to depend upon how rapidly a line goes to open circuit, which is controlled by the current density. Open-circuit failure tends to occur in regions where the damage has become extremely severe, presumably where the local cross-sectional area has become so reduced that localized melting takes place. The selectivity in damage locations suggests that the process is very dependent upon the nature of the particular grain arrangement within the line. The EBSD results indeed show such a dependence.

In addition to the pronounced development of topography, we observed two major microstructural changes in the course of damage evolution induced during AC testing of these lines: grain growth and grain re-orientation. Both of these changes occurred in a spatially selective manner, similar to the formation

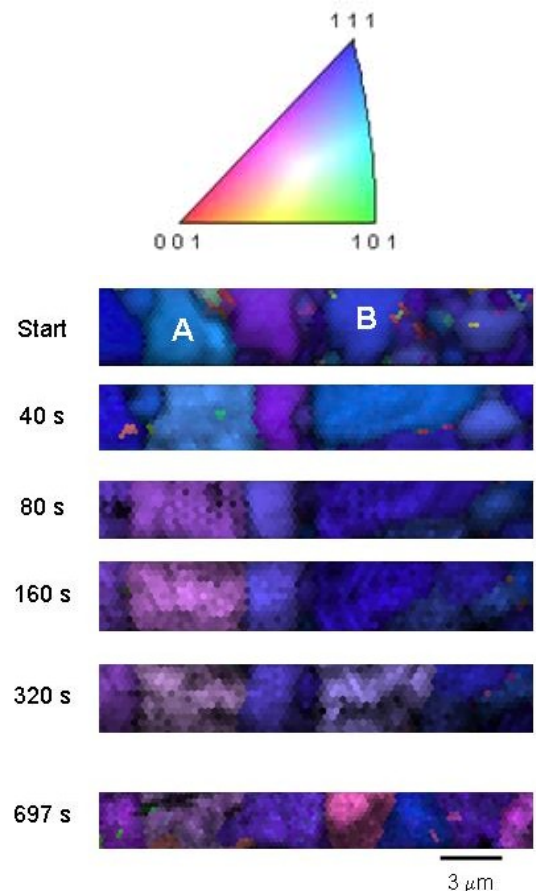


Figure 4. Top: Inverse pole figure legend to colors. Bottom: Series of automated EBSD orientation maps corresponding to SEM images of Figure 3. Magnifications of the two figures are the same. Colors represent crystallographic directions corresponding to specimen normal.

of surface topography. Figure 4 shows a series of EBSD orientation maps taken from the identical regions shown in Figure 3. The colors in this series represent crystallographic directions lying along the specimen normal direction. The as-deposited structure is typical of physical vapor-deposited metals on oxidized silicon, namely there is a strong (111) fiber texture, with nearly equiaxed grains. Pole figures from thousands of grains show that nearly all grains have surface normals within 10 degrees of $\langle 111 \rangle$ in the as-deposited condition. Figure 4 shows the two additional predominant microstructural changes induced by AC stressing. The grains marked “A” and “B” each show growth followed by re-orientation of the surface normal. Both effects can also be seen in Figure 5, which shows a series of orientation maps with colors representing crystallographic directions lying along the specimen longitudinal direction. As expected, grains “A” and “B” show re-orientation in this direction, also. In contrast, the grains lying between grains “A” and “B” undergo little re-orientation and also show little surface deformation. The orientation changes can be tracked on inverse pole figures, as shown in Figure 6. Data points that showed relatively large re-orientations are highlighted in black. We note that progressively larger populations of points shifted further from the starting (111) normal orientation as testing progressed. Similarly, in the longitudinal direction, progressively larger populations of points shifted from the range of single slip band orientations, shown at the start of the test, toward (001).

DISCUSSION

The major changes we observed during AC stressing of these Al-1Si lines to open-circuit failure were the formation of severe topography and the growth and re-orientation of grains.

Deformation and Topography

Estimates of the stress amplitude associated with AC testing at these current densities can be made by assuming all

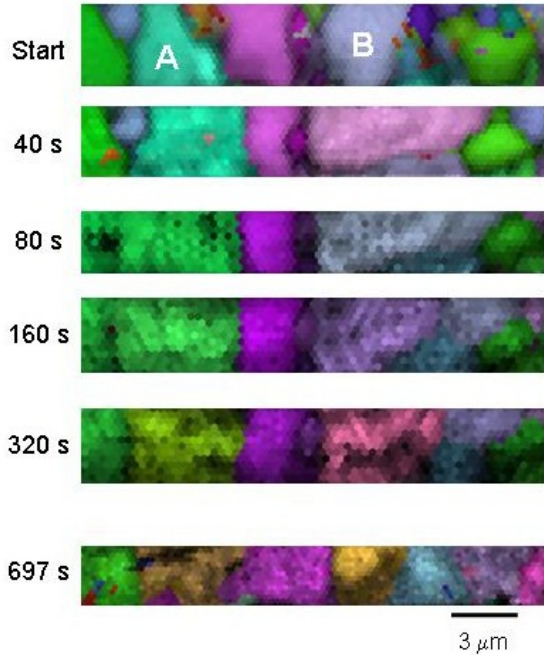


Figure 5. Series of automated EBSD orientation maps corresponding to SEM images of Figures 3 and 4. Magnifications of the figures are the same. Colors represent crystallographic directions corresponding to longitudinal specimen direction. See Figure 4 for color legend.

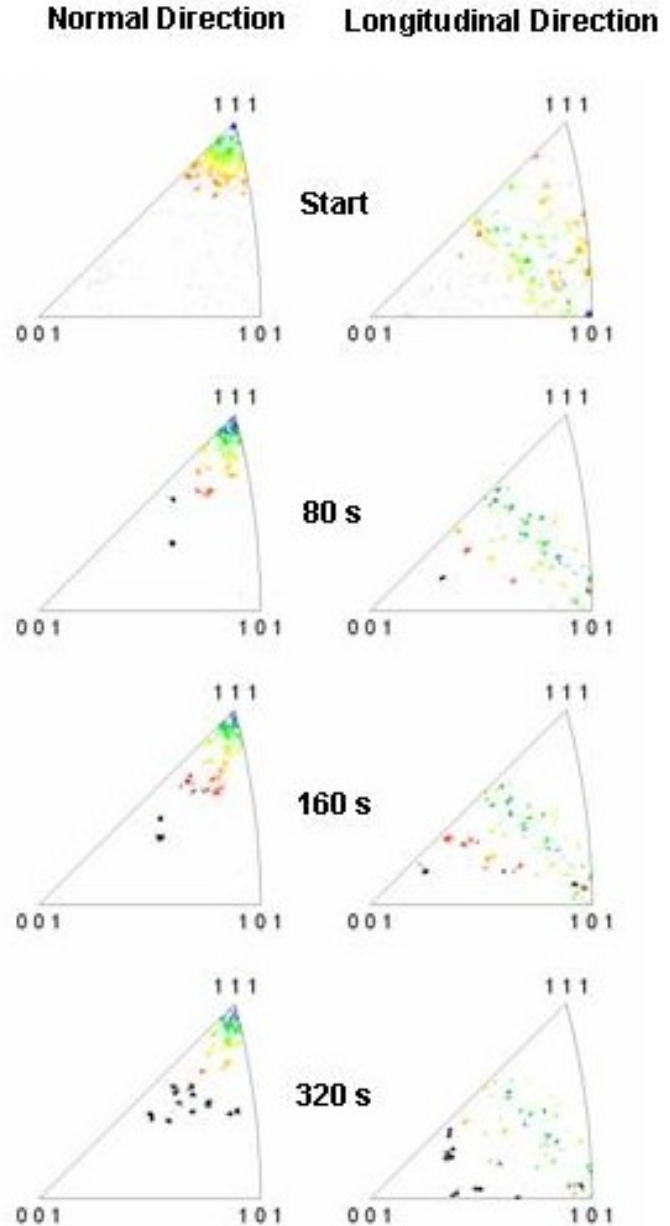


Figure 6. Series of inverse pole figures (IPFs) showing grain re-orientation with time induced by AC stressing. The data in these IPFs was taken from the same area as that mapped in Figures 4 and 5. Black data points are from grain that underwent large re-orientations.

the power input into a line is dissipated entirely in the form of heat. A calibration of line resistivity versus temperature in combination with time-resolved resistance measurements [8] suggested that the temperature amplitude associated with a cyclic current density of 10 MA/cm² was approximately 100 K. While we did not make time-resolved resistance measurements from the particular specimen studied with EBSD, we can assume the temperature cycle to be at least 100 K as well, since we applied a 20 % higher current density. Such a temperature change corresponds to a thermal-mismatch stress of approximately 210 MPa, using the usual values for elastic constants. X-ray diffraction showed a residual biaxial deposition stress of 270 MPa prior to testing [8]. We note also that the chip temperature was less than 10K above room temperature, corresponding to an rms decrease in the residual tensile film stress of less than approximately 21 MPa. Considering the effect of the slightly increased chip temperature, we may assume the lines to have been under an rms stress of approximately 250 MPa in tension, onto which the cyclic stress was superimposed. So, we expect the lines to cycle approximately between 250 and 40 MPa during each AC half-cycle. Such a stress amplitude may exceed the monotonic yield strength for thin film aluminum on a constraining substrate.

Surface topography, presumably corresponding to slip activity, was observed within the first minute of testing, or in less than 12,000 thermal cycles. The determination of which grains will deform depends on a combination of several factors. Among these are the value of the resolved shear stress within a given grain, and the diameter of that grain. Both of these factors control the localized strength of that grain. In general, we found that initially larger grains often exhibited the first signs of deformation, consistent with a locally distributed Hall-Petch type of behavior. That is, within a polycrystalline array, those grains of larger size and lower strength are likely to deform first. As cycling continues, grains that have already begun to deform plastically tend to continue to deform with increasing severity, as illustrated in Figure 3. EBSD analysis revealed that virtually all of the linear traces on the surface of the line correspond to <112> directions, as has been seen previously with persistent slip bands in another high stacking fault energy material, nickel [10]. The process, however, is not simply dependent upon the starting microstructure. We must also consider the observations of grain growth and re-orientation.

Grain Growth and Grain Re-orientation

The growth and re-orientation of grains during cycling suggests that some type of annealing process is occurring simultaneously with deformation. The inverse pole figures of Figure 6 indicate that the surface normal directions of some grains move away from the <111> pole typical of the as-deposited structure towards the <001> pole. Similarly, the longitudinal orientations of some grains move away from the typical single slip distribution associated with initially a

random in-plane texture, towards the <001> pole. However, a true cube texture typical of the full recrystallization of face-centered cubic materials was never fully attained. We have, though, found isolated grains that were nearly perfectly cube-oriented after extensive AC stressing. This behavior is general and very repeatable.

While the trend towards a recrystallization texture may be suggested, we believe that true recrystallization is not occurring for three reasons. First, it is unlikely that even the localized temperature becomes high enough for this to occur. For 99 % pure or lightly alloyed aluminum, the one-hour recrystallization temperature ranges from approximately 240 to 320 °C [11], depending on grain size and deformation. We estimate the peak temperature within an AC half-cycle to be only slightly higher than 100 °C, and the total time at that peak temperature for the test under consideration is only a matter of seconds. It is unlikely that recrystallization could occur under such poor thermal conditions. Second, the orientation changes we observed evolved with increased cycling, in contrast to the case where a population of new grains nucleates. Similarly, the new orientations are not the result of the growth of a certain population of pre-existing grains with some preferred orientation. We can in fact track the re-orientation of particular grains. It is not uncommon to find orientations changing by as much as 35 degrees. Third, in grains that show growth and re-orientation, we observe significant surface deformation that becomes more severe with increased cycling, which is inconsistent with the formation of new crystals.

Our final points address some preliminary assessments of the structure of grain boundaries and the degree of lattice perfection as determined by EBSD patterns. First, there seems to be no apparent dependence of grain growth on boundary type, since most of the grain boundaries in the as-grown structure were tilt boundaries. Also, at first glance, both high- and low-angle boundaries behave similarly. Second, EBSD pattern quality is retained throughout testing in many grains, even those that have undergone extremely severe deformation. This suggests that there remain few defects in the material even after many cycles. The processes we have observed could be considered some unusual form of recovery.

ACKNOWLEDGMENTS

We thank the NIST Office of Microelectronics Programs for support. This work is a contribution of the U.S. Department of Commerce; it is not subject to copyright in the United States.

REFERENCES

1. W. D. Nix, "Mechanical Properties of Thin Films," *Metall. Trans.* 20A, 2217-2245 (1989).
2. C. Laird, P. Charsley, and H. Mughrabi, "Low Energy Dislocation Structures Produced by Cyclic Deformation," *Mater. Sci. Eng.* 81, 433-450 (1986).
3. T. Foecke and D. vanHeerden, "Experimental Observations of Deformation Mechanisms in Metallic Nanolaminates," *Chemistry and Physics of Nanostructures*

and Related Non-Equilibrium Materials, eds. E. Ma *et al.*, TMS, 193-200 (1997).

4. G. Dehm and E. Arzt, "In-situ Transmission Electron Microscopy Study of Dislocations in a Polycrystalline Cu Thin Film Constrained by a Substrate," *Appl. Phys. Lett.* 77, 1126-1128 (2000).
5. R. Schwaiger, G. Dehm, and O. Kraft, "Cyclic deformation of polycrystalline Cu films," *Phil. Mag.* 83, 693-710 (2003).
6. P. A. Flinn, "Principles and Applications of Wafer Curvature Techniques for Stress Measurements in Thin Films," *Mat. Res. Soc. Symp. Proc.* 130, eds. J. C. Bravman *et al.*, 41-51 (1989).
7. R. Mönig, R. R. Keller, and C. A. Volkert, "Thermomechanical Fatigue Testing of Thin Metal Films," *Rev. Sci. Instrum.*, in press (2004).
8. R. R. Keller, R. Mönig, C. A. Volkert, E. Arzt, R. Schwaiger, and O. Kraft, "Interconnect Failure due to Cyclic Loading," *Stress-Induced Phenomena in Metallization: Sixth International Workshop*, eds. S. P. Baker *et al.*, Amer. Inst. Phys., 119-132 (2002).
9. R. H. Geiss, A. Roshko, K. A. Bertness, and R. R. Keller, "Electron Backscatter Diffraction for Studies of Localized Deformation," *Electron Microscopy: Its Role in Materials Science*, eds. J. R. Weertman *et al.*, TMS, 329-336 (2003).
10. M. Hollmann, J. Bretschneider, and C. Hoste, "Dislocation Structure and Strain Localization in Nickel Single Crystals Cyclically Deformed at 77 K," *Cryst. Res. Technol.* 35, 479-492 (2000).
11. J. D. Verhoeven, *Fundamentals of Physical Metallurgy*, Wiley: New York, p. 351 (1975).